Applied Catalysis B: Environmental 126 (2012) 64–75

Contents lists available at SciVerse ScienceDirect

Applied Catalysis B: Environmental

journal homepage: www.elsevier.com/locate/apcatb

Catalytic combustion of chlorobenzene over Ru-doped ceria catalysts

Qiguang Dai, Shuxing Bai, Zhengyi Wang, Xingyi Wang*, Guanzhong Lu*

Lab for Advanced Materials, Research Institute of Industrial Catalysis, East China University of Science and Technology, Shanghai 200237, PR China

ARTICLE INFO

Article history:
Received 17 April 2012
Received in revised form 7 July 2012
Accepted 16 July 2012
Available online 22 July 2012

Keywords:
Chlorobenzene
Ceria
Ru
Catalytic combustion
Chlorinated hydrocarbons

ABSTRACT

CeO_2 and Ru doped CeO_2 nanoparticles with small particle sizes (~7 nm) and high surface area (~100 $m^2 g^{-1}$) were prepared by a simple precipitation/coprecipitation method and aqueous NaOH solution (10 wt%) as the precipitating agent, and characterized by XRD, N_2 adsorption, TEM/HRTEM, Raman, XPS and H_2-TPR. The catalytic combustion of chlorobenzene (CB) was investigated for the first time. The results revealed that the Ru doped CeO_2 catalysts exhibit an outstanding catalytic activity ($T_{90\%}$ below 250 °C) and stability (at least 82 h at 275 °C) for CB decomposition. The better stability of the Ru-CeO_2 catalysts can be ascribed to the inorganic chlorine species or dissociative Cl adsorbed on active sites can be removed rapidly via the Deacon process catalysized by RuO_2 component with extraordinary stability (limited chlorination and easier Cl_2 evolution).

1. Introduction

Chlorinated hydrocarbons (CHCs), mainly including dichloromethane (DCM), trichloroethylene (TCE), perchloroethylene (PCE), vinyl chloride (VC), 1,2-dichloroethane (DCE) and chlorobenzene (CB), are widely used in industries as solvents, dry-cleaning agents, degreasing agents, and intermediates in the production of plastics, synthetic resins or pharmaceuticals. However, these compounds are considered one of main categories of air pollutants due to their direct (toxic and carcinogenic) and indirect (photochemical smog) environmental effects. Therefore, many technologies have been investigated for the removal of CHCs, such as thermal combustion, catalytic combustion, photocatalytic degradation, catalytic hydrodechlorination, adsorption, pervaporation and biofiltration. Among these methods, low temperature catalytic combustion appears to be one of the most promising and effective technologies for CHCs abatement.

In the past two years, a considerable amount of effort has been concentrated in the research work on the catalytic combustion of CHCs [1–23], in which catalysts employed were mainly the following types: pure ceria [1], MnO_x–CeO_2 mixed oxide [2–4], CeO_2-modified USY zeolite [5], cerium-zirconium solid solution [6], Fe-zeolites/doped zirconia catalysts [7–9], Co_3O_4 [10], supported V_2O_5 [11–15], CrO_x [16,17], MnO_x [18–21] and PdO_x [16,22]. Among those, the ceria-based catalysts continue to attract attention because of their high activity and co-catalysis for other catalysts (such as transition metal oxides and solid acid catalysts). Since 2002, our group has been engaged in the research about low-temperature catalytic combustion of TCE and CB over pure CeO_2 [1,24–27] and transition metals-doped CeO_2 [2–4,28–30] catalysts. It was found that CeO_2 presents high activity for catalytic destruction of various chlorinated hydrocarbons, which is attributed to high dissociation ability for C—Cl bonds, oxygen mobility and abundant oxygen defects of CeO_2. However, the deactivation of CeO_2 is very fast due to the strong adsorption of inorganic chlorine species or dissociative Cl produced from the decomposition of CHCs on active sites. We found in the further studies that the introduction of transition metals (such as Fe, Co, Cu, Ni and Mn), especially Mn, can improve evidently both the activity and stability of pure CeO_2 catalysts. The high stability of transition metals-doped ceria catalysts derives from that the adsorbed inorganic chlorine species or dissociative Cl can be removed rapidly from the sufface or active sites of CeO_2 via the formation and reoxidization of intermediate TMO_yCl_x or $TMCl_x$. Zhou [5,31,32] investigated the deep oxidation of DCE over CeO_2-modified Y zeolites (including CeO_2/USY, CeO_2/HY and CeO_2/SSY), and the results showed that the catalytic activity of the supported CeO_2 catalysts was much higher than that of Y zeolites, and in particular, CeO_2/USY exhibited the highest activity. Zhou considered that both acidity and redox property play important roles in the DCE decomposition, and the synergy between CeO_2 species and USY zeolite shows an enhancement in the catalytic activity. Gutiérrez-Ortiz and co-workers [6,33,34] studied continuously the oxidation of CHCs (such as DCE and TCE) over cerium zirconium solid solution catalysts in recent years. The Ce/Zr mixed oxide catalysts exhibited the activities dependent on Ce/Zr molar content, and the selectivity toward CO_2 and Cl_2 was found to be noticeably promoted with increasing cerium

* Corresponding authors. Tel.: +86 21 64253183; fax: +86 21 64253372.
E-mail addresses: daiqg@ecust.edu.cn (Q. Dai), wangxy@ecust.edu.cn (X. Wang), gzhlu@ecust.edu.cn (G. Lu).

0926-3373/$ – see front matter © 2012 Elsevier B.V. All rights reserved.
http://dx.doi.org/10.1016/j.apcatb.2012.07.008

content. They owed the high activity to a suitable combination of a large population of acid sites, easily accessible oxygen species and hydrophobic nature (attributable to cerium content) of Ce/Zr mixed oxides. Additionally, Pitkäaho et al. [35] investigated the oxidation of PCE over Pt, Pd, Rh and V_2O_5 catalysts supported on Al_2O_3, and found that the addition of TiO_2 or CeO_2 into Al_2O_3 enhanced evidently catalysts' efficiency, and the activity of Pt/Al_2O_3-CeO_2 and Pd/Al_2O_3-CeO_2 catalysts were superior to the other tested catalysts. Authors considered that the strong synergistic effect between metal and support together with improved redox properties might be explanations for higher catalytic activity. The above studies indicate that ceria-based catalysts are very suitable and potential catalysts for catalytic combustion of CHCs, though there are still many problems remained to be further understood and resolved, such as the stability at low temperature.

As we all know, Ru-based catalyst has been industrially implemented for large-scale chlorine production via HCl oxidation (Deacon Process), due to its higher reactivity (favored reoxidation, 180–500 °C), extraordinary stability (limited chlorination and resistant against HCl and Cl_2 exposure) and easier Cl_2 evolution [36–42]. According to our previous work [25,26], it is necessary to remove or transfer rapidly the inorganic chlorine species or dissociative Cl from the active sites in order to improve the stability of CeO_2 catalysts. Hereby, it is speculated that the introduction of ruthenium possibly improves the ability of CeO_2 resistant to Cl species poisoning. Additionally, RuO_2 has received considerable attention as a heterogeneous catalyst in oxidation of various organic compounds, among others such as carbon monoxide [43], soot [44] and methane [45]. Recently, several research groups studied the performances of Ru-based catalysts in TCE catalytic combustion. Lee and Yoon [46,47] reported that Cr-oxide catalysts promoted with a small amount of Ru (0.4 wt.%) present high activity, low selectivity for CO and a decreased propensity for deactivation in catalytic combustion of TCE. Miranda [48] also investigated the performance of 0.5%Ru/Al_2O_3 for the severe oxidation of TCE, and found that the activity of Ru catalysts is higher than some other catalysts.

However, to the best of our knowledge, studies on catalytic combustion of CHCs over Ru-doped or supported CeO_2 catalyst has not been reported yet. Hence, this work is focused on the study of the performance of Ru-doped CeO_2 catalyst for CHCs catalytic combustion, and in particular CB catalytic combustion.

2. Experimental

2.1. Catalysts preparation

CeO_2 and Ru-CeO_2 catalysts were prepared by precipitation/coprecipitation method using NaOH as the precipitating agent. In preparation of CeO_2, 10 g of $Ce(NH_4)_2(NO_3)_6$ and 7.5 g of NaOH were dissolved in 25 mL and 50 mL of deionized water, respectively. Then NaOH solution was quickly added to $Ce(NH_4)_2(NO_3)_6$ solution and stirred at room temperature for 2 h. Subsequently, the mixture was placed statically for 48 h at room temperature; the precipitates were washed with distilled water and ethanol, then dried at 80 °C for 12 h and calcined in air at 450 °C for 3 h. For Ru-CeO_2, the same recipe except for the addition of ruthenium precursor, was obtained by adding a given amount of ruthenium chloride solution (the content of ruthenium is 0.02 g mL^{-1}) to $Ce(NH_4)_2(NO_3)_6$ solution.

Additionally, Ru/CeO_2 and Ru/SBA-15 samples were prepared by incipient-wetness impregnation method, among which CeO_2 was prepared by the above method and SBA-15 (BET surface area 506 $m^2\,g^{-1}$) purchased from Shanghai Boyle Chemical Co., Ltd. The support CeO_2 or SBA-15 was impregnated with an aqueous solution containing an appropriate amount of ruthenium chloride, and then dried at 80 °C for 12 h and calcined in air at 450 °C for 3 h.

2.2. Catalysts characterization

2.2.1. X-ray diffraction

The powder X-ray diffraction patterns (XRD) of samples were recorded on a Rigaku D/Max-rC powder diffractometer using Cu Kα radiation (40 kV and 100 mA). The diffractograms were recorded in the 2θ range of 10–80° with a 2θ step size of 0.01° and a step time of 10 s.

2.2.2. Nitrogen adsorption/desorption

The nitrogen adsorption and desorption isotherms were measured at 77 K on an ASAP 2400 system in static measurement mode. Samples were outgassed at 160 °C for 4 h before the measurement. The specific surface area was calculated using the BET model.

2.2.3. X-ray fluorescence spectroscopy

Ruthenium content was determined by X-ray fluorescence (XRF) using a Shimadzu (XRF-1800) wavelength dispersive X-ray fluorescence spectrometer. Samples were pressed as homogeneous tablets (ϕ20 mm) of compressed (30 MPa) powder of the catalyst systems.

2.2.4. Transmission electron microscopy

The TEM images of the powder samples were recorded on a JEM-1400 instrument operated at 120 kV. High-resolution transmission electron microscopic (HRTEM) images were taken on a JEM-2100 field emission transmission electron microscope that operated at 200 kV.

2.2.5. Raman spectroscopy

The Raman spectra were obtained on a Renishaw in Viat + Reflex spectrometer equipped with a CCD detector at ambient temperature and moisture-free conditions. The emission line at 514.5 nm from an Ar^+ ion laser (Spectra Physics) was focused, analyzing spot about 1 mm, on the sample under the microscope. The power of the incident beam on the sample was 3 mW. Time of acquisition was varied according to the intensity of the Raman scattering. The wave numbers obtained from spectra were accurate to within 2 cm^{-1}.

2.2.6. Temperature programmed reduction

H_2-temperature programmed reduction (H_2-TPR) of samples (100 mg) placed at the bottom of the U-shaped quartz tube was investigated by heating samples in H_2 (5 vol.%)/Ar flow (30 mL min^{-1}) at a heating rate of 10 °C min^{-1} from 50 to 600 °C. The hydrogen consumption was estimated on the basis of the analysis with a thermo-conductivity detector (TCD), the extent of reduction was quantitatively calculated according to the TPR peak areas and the result was calibrated on the basis of the hydrogen consumption from the reduction of CuO to Cu.

2.2.7. X-ray photoelectron spectroscopy

The XPS measurements were made on a VG ESCALAB MK II spectrometer by using Mg Kα (1253.6 eV) radiation as the excitation source. Charging of samples was corrected by setting the binding energy of adventitious carbon (C1s) at 284.6 eV. The powder samples were pressed into self-supporting disks, loaded into a sub-chamber, and evacuated for 4 h, prior to the measurements at 298 K.

2.3. Catalytic activity measurement

Catalytic combustion reactions were carried out in a continuous flow microreactor constituted of a U-shaped quartz tube of 3 mm of inner diameter at atmospheric pressure. 200 mg catalyst

was placed at the bottom of the U-shaped micro-reactor. The feed flow through the reactor was set at 40 cm^3 min^{-1} and the gas hourly space velocity (GHSV) was maintained at 15,000 h^{-1}. Feed stream to the reactor was prepared by delivering liquid CB with a syringe pump into dry air, which was metered by a mass flow controller. The injection point was electrically heated to ensure complete evaporation of the liquid reaction feeds. The concentration of CB in the reaction feeds was set at 550 ppm. The temperature of the reactor was measured with a thermocouple located just at the bottom of the microreactor. The effluent gases were analyzed by an on-line gas chromatograph equipped with a FID detector. Catalytic activity was measured over the range 100–350 °C and conversion data were calculated by the difference between inlet and outlet concentrations. Conversion measurements and product profiles were taken after maintained for 5 min at each test temperature. Additionally, mass spectrum was used for the determination of the main intermediates and by-products.

The temperature-programmed surface reaction (TPSR) measurement was carried out under the conditions as the same as that in the catalytic activity tests in order to detect the reactants and products in effluence. First, the feeding air stream containing a certain concentration of CB (such as 1500 ppm) flowed through the catalyst bed at 100 °C. After the adsorption–desorption of CB reached an equilibrium, the catalyst bed was heated from 100 to 200 °C or 275 °C at 10 °C min^{-1}. Reactants and products in effluence were analyzed on-line by mass spectrometer apparatus (HIDEN QIC-20).

3. Results and discussion

3.1. Catalyst characterization

The phase structures of the samples were investigated by XRD. As shown in Fig. 1, all samples except for 1%Ru/SBA-15 exhibit only the characteristic peaks of the cubic fluorite structure of CeO_2 at 28.7°, 33.1°, 47.4°, 56.3°, 69.7°, and 76.9°. No crystalline phase ascribed to ruthenium oxide can be found. A possible reason can be that the ruthenium species dispersed well on the surface of CeO_2 nanoparticles or incorporated into the CeO_2 lattice to form solid solution. Additionally, the average crystallite sizes of as prepared samples can be calculated by applying the Debye–Scherrer formula on the CeO_2 (1 1 1) diffraction peaks and lattice parameters are listed in Table 1. According to the Table 1, crystallite sizes and lattice parameters of CeO_2 decrease with the introduction of Ru, and the decrease in the lattice parameter distinctly indicated the incorporation of Ru into the CeO_2 lattice due to the ionic radius of Ru is smaller than that of Ce. For the 1%Ru/SBA-15 sample, the characteristic peaks of RuO_2 at 27.9°, 34.8° and 54.2° can be observed.

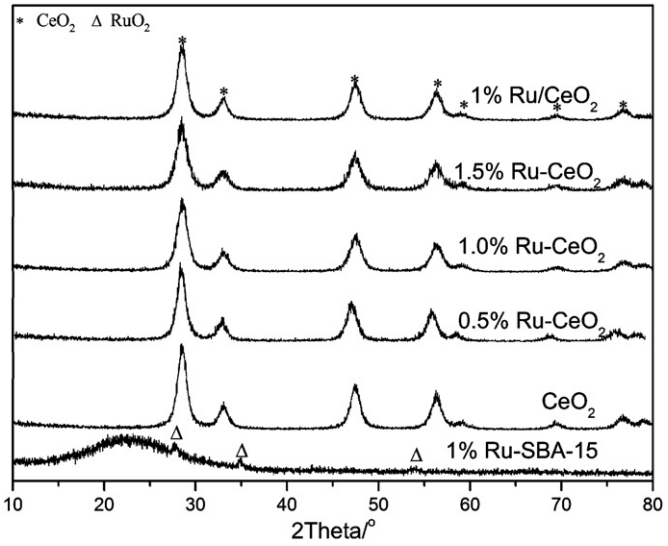

Fig. 1. XRD patterns of Ru based and CeO_2 catalysts.

Fig. 2 showed Raman spectra of the samples. All Ce-based samples present a strong band at about 460 cm^{-1}, which is attributed to the Raman-active vibrational mode (F_{2g}) of fluorite-type structure. It can be considered as a symmetrical stretching vibration of the oxygen atoms around cerium ions. Furthermore, another weak band appears at around 600 cm^{-1}, which is related to oxygen vacancies due to the presence of Ce^{3+} ions in CeO_2 lattice. For the Ru-or/CeO_2 samples, there are two very weak and broad bands at 320 and 710 cm^{-1}, which are attributed to RuO_2 [49]. For the 1%Ru/SBA-15, the three major Raman bands, namely E_g, A_{1g}, and B_{2g} modes of RuO_2 are located at about 400, 520, and 640 cm^{-1}, respectively, but the values distinctly shift to lower wave number compared with the reported values in the literature (which are located at about 523, 646, and 710 cm^{-1}, respectively) [49].

TPR profiles of Ru based and pure CeO_2 catalysts were shown in Fig. 3. As 1%Ru/SBA-15 catalyst has only one reduction peak at 165 °C, Ru in RuO_2 changed directly from Ru^{4+} to Ru^0 without forming intermediate valence states such as Ru^{3+} or Ru^{2+}. All Ru- or/CeO_2 catalysts exhibit one sharp reduction peak around 130 °C except a broad reduction peak at 275–450 °C, the former is attributed to the reduction of ruthenium oxide and the latter is corresponded to surface oxygen species of cerium oxide. Additionally, the pure CeO_2

Table 1
Surface and structural properties of Ru based and pure CeO_2 catalysts.

Catalyst	Ru content[a]	S_{BET} (m^2 g^{-1})[b]	Crystallite size (nm)[c]	Lattice parameters (nm)[d]	Particle size (nm)[e]	H_2 consumption (μmol/g cat)[f]		
						Ru		Ce
						Theoretical	Actual	
CeO_2	0	100.8	7.4	0.5413	5–6	–	–	410
0.5%Ru-CeO_2	–	107.2	7.5	0.5418	–	–	607	283
1.0%Ru-CeO_2	0.58	105.0	6.5	0.5379	6–7	115	738	239
1.5%Ru-CeO_2	1.01	99.3	6.6	0.5394	–	200	796	209
1.0%Ru/CeO_2	1.14	82.4	6.8	0.5387	–	226	740	84
1.0%Ru/SBA-15	0.98	452	–	–	–	194	184	–
1.0%Ru-CeO_2-D	–	–	–	–	–	115	785	364
1.0%Ru-CeO_2-R	–	–	–	–	-	115	619	34

[a] Ru content measured by XRF.
[b] BET surface area.
[c] The crystallite sizes of the CeO_2 (1 1 1) were calculated from X-ray diffraction line broadening using the Scherrer equation.
[d] Lattice parameters calculated from XRD results.
[e] Particle size obtained from TEM.
[f] Calculated from TPR results.

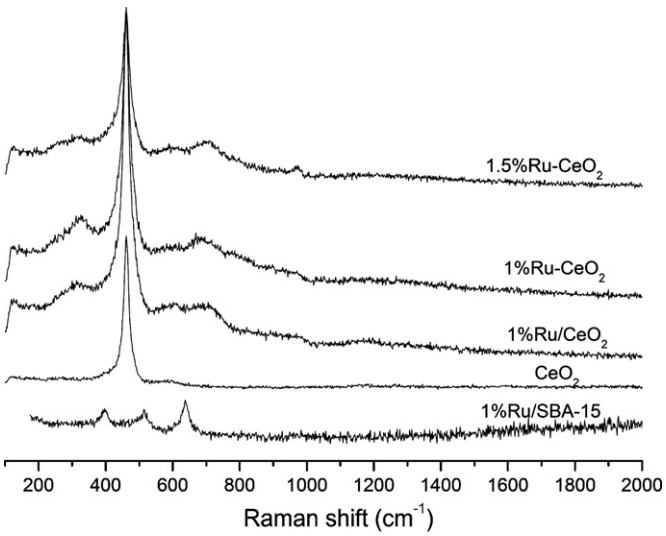

Fig. 2. Raman spectra of Ru based and CeO_2 catalysts.

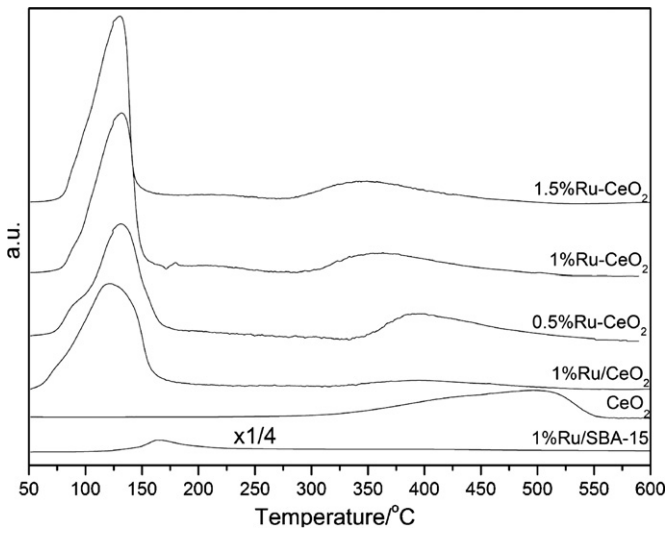

Fig. 3. TPR profiles of Ru based and CeO_2 catalysts.

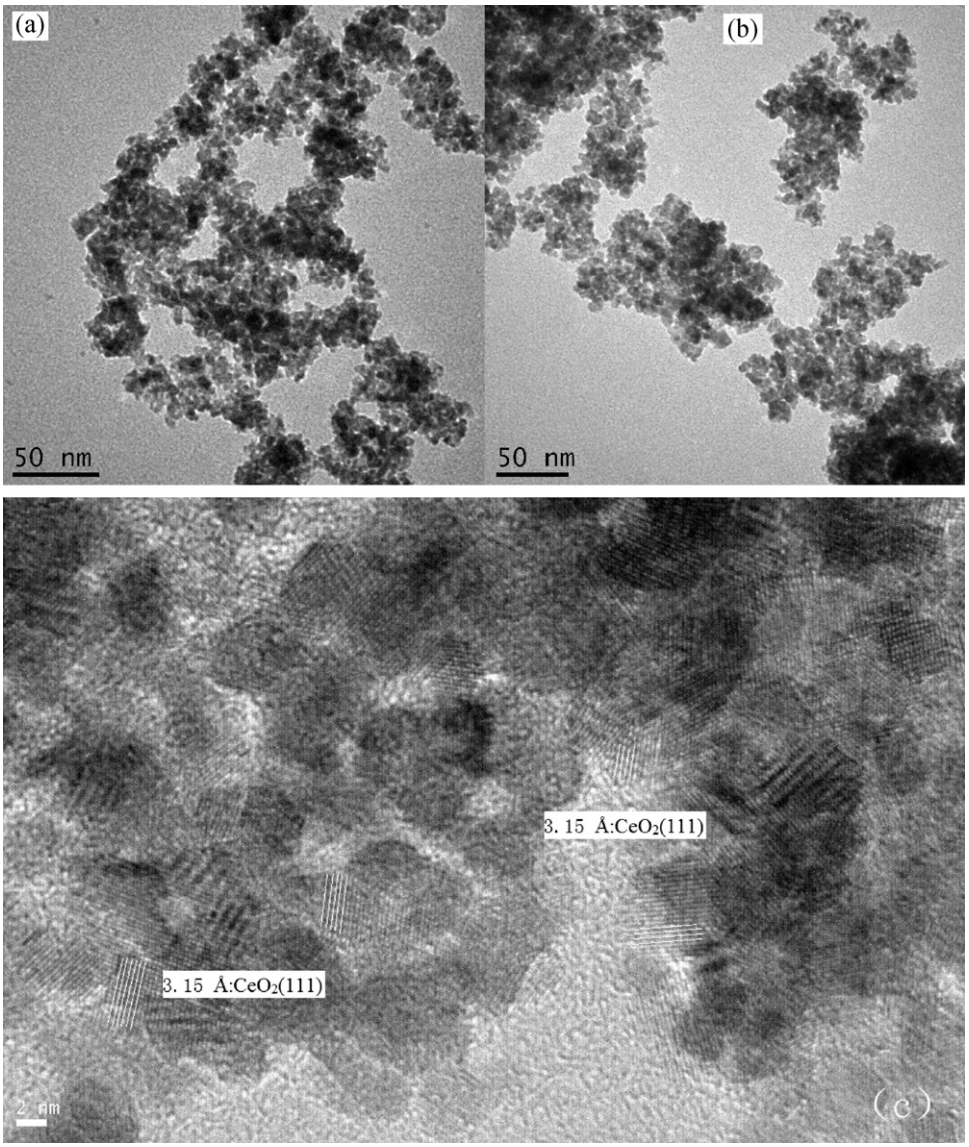

Fig. 4. TEM images of CeO_2 (a), 1%Ru-CeO_2 (b), and HRTEM image of 1%Ru-CeO_2 (c).

has a broad peak in a temperature range from 325 to 550 °C and the maximum peak is around 500 °C. It can be seen that the reduction temperature of RuO_2 or CeO_2 in Ru- or/CeO_2 catalysts shift to lower temperature ranges, which is consistent with Jacobs et al. [50] and Wang et al. [51]. Moreover, the reduction temperature of CeO_2 shifts to lower temperature with the increase of Ru content doping CeO_2, for example, the reduction temperature decreases from 400 °C of 0.5%Ru-CeO_2 to 340 °C of 1.5%Ru-CeO_2. Furthermore, the amounts of hydrogen consumption of all catalysts during TPR measurement are summarized in Table 1. The amount of hydrogen required for the reduction was calculated on the basis of the following theoretical hydrogen consumption: $RuO_2 + 2H_2 \rightarrow Ru^0 + 2H_2O$. For Ru- or/$CeO_2$ catalysts, the amount of hydrogen consumed during the reduction of RuO_2 is much higher than the theoretical value (H_2/Ru ratio = 2) and it could be probably due to spill over hydrogen from the metal to the support [51]. Correspondingly, the ratio value of 1.0%Ru/SBA-15 is only 1.86. Additionally, it can be found that the amount of H_2 consumed by CeO_2 (the peaks at 275–450 °C) in Ru- or/CeO_2 catalysts is lower than the pure CeO_2 (410 μmol/g cat), which also indicates the partial surface oxygen in CeO_2 is migrated to RuO_2. Another possible reason is that the Ru species dispersed on the surface of CeO_2 occupied partial adsorbed sites of oxygen, which can result in the decrease of surface oxygen species.

Fig. 4a and b show the typical TEM image of CeO_2 and 1%Ru-CeO_2 samples. The pure CeO_2 (Fig. 2(a)) and 1%Ru-CeO_2 (Fig. 2(b)) nanoparticles have irregular shape and about 5–6 nm and 6–7 nm mean diameter, respectively. This value is in good agreement with the average mean diameter which arise from the application of the Scherrer equation on the XRD data (~7.4 nm and ~6.5 nm). Fig. 4c shows a typical HRTEM image of 1%Ru-CeO_2 sample, which clearly shows the lattice fringes of the CeO_2 (the d-spacing of 3.15 Å is due to (1 1 1) plane of the CeO_2). However, no obvious RuO_2 nanoparticles can be observed and crystalline RuO_2 lattice fringes also are very difficult to be found due to the poor crystallinity of the as-grown RuO_2 nanoparticles. This is consistent with the XRD results.

Fig. 5(a)–(d) present XPS spectra of Ce 3d, Ru 3d and O1s obtained from CeO_2 and 1%Ru-CeO_2 catalysts. The widely acceptable interpretation of Ce 3d XPS spectrum of CeO_2 is that it consists of 10 Gaussian-like contributions [52], arising from various oxidation states and multiplet splitting. Of these, six peaks arise from Ce^{4+} contributions and four from Ce^{3+}. The peaks at 884.1, 889.0, 897.8, 900.0, 908.1 and 917.3 eV are attributed to Ce^{4+}, while the four peaks at 881.4, 885.1, 898.2 and 902.8 eV are typical for Ce^{3+}. The calculated concentration of Ce^{3+} ($[Ce^{3+}]$) of the synthesized CeO_2 was semiquantitatively analyzed using the integrated peak area of the respective valence states using the following equation [53]:

$$[Ce^{3+}]\% = \frac{A_{v_0} + A_{v'} + A_{u_0} + A_{u'}}{A_v + A_{v''} + A_{v'''} + A_u + A_{u''} + A_{u'''}} \times 100\%$$

Values of $[Ce^{3+}]$ of pure CeO_2 and 1%Ru-CeO_2 are estimated to be ~18.3% and ~11.8%, respectively. It can be found that the introduction of Ru decreases the value of $[Ce^{3+}]$ in CeO_2, which also demonstrates the reduction of the oxygen vacancies. On XPS spectrum (Fig. 4b) of C1s-Ru 3d, the two peaks at 281.8 and 283.0 eV in the Ru 3d5/2 region and the corresponding peaks in the Ru 3d3/2 at 285.9 and 287.1 eV are ascribed to hydrated RuO_2 and Ru^{6+}, respectively [54]. The spectrum of O1s has a single peak at 529.3 eV, which is assigned to lattice oxygen. Two shoulder peaks at ca. 531 and 533 eV are observed, which can be attributed to the adsorbed oxygen or/and weekly bonded oxygen species [55], or to surface oxygen in the form of hydroxyl species and/or adsorbed water species as contaminants at the surface. Moreover, the content of surface oxygen species at 531 eV in 1%Ru-CeO_2 is higher than that of pure CeO_2, which indicates that the 1%Ru-CeO_2 probably possesses higher oxidation performance.

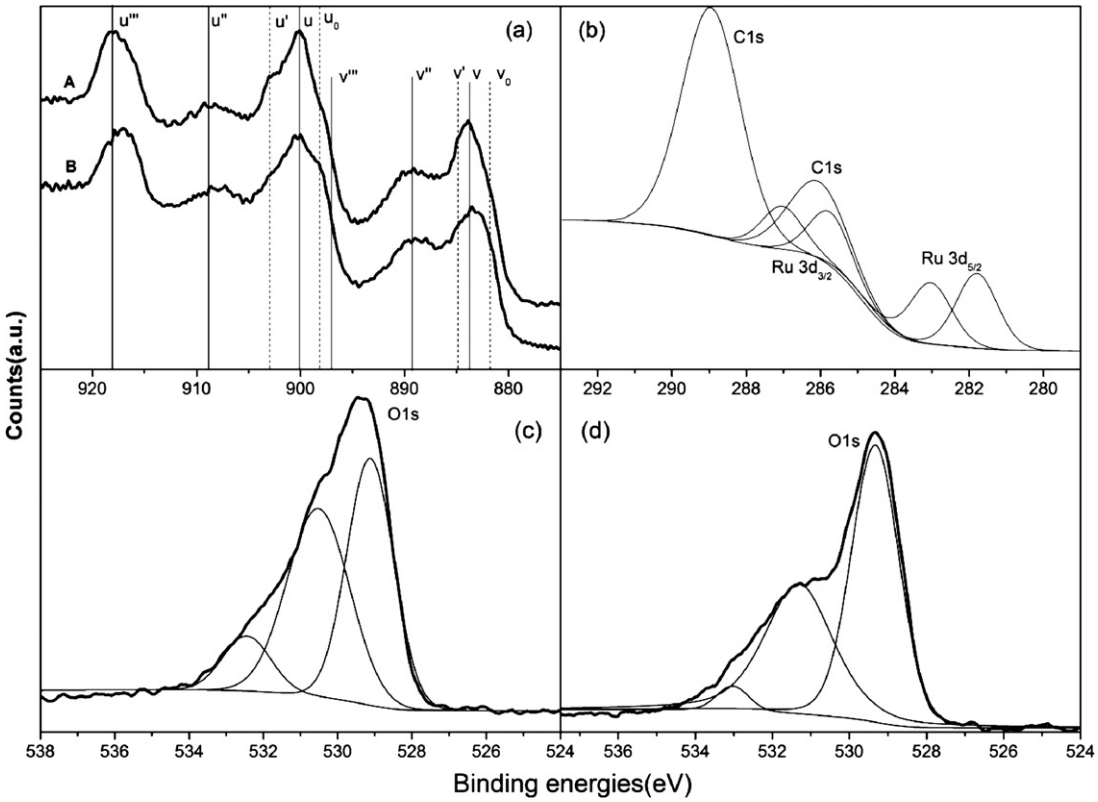

Fig. 5. XPS spectra of CeO_2 and 1%Ru-CeO_2 catalysts: (a) Ce 3d XPS spectra of CeO_2 (A) and 1%Ru-CeO_2 (B); (b) peak fitting of C1s and Ru 3d for 1%Ru-CeO_2; (c) O1s spectrum of CeO_2; (d) O1s spectrum of 1%Ru-CeO_2.

3.2. Catalytic activity

The catalytic combustion of CB was studied over Ru-based and pure CeO_2 catalysts and the experimental results are listed in Fig. 6. Compared with 1%Ru/SBA-15 catalyst, CeO_2-based catalysts evidently show higher activities, and the complete oxidation of CB is achieved below 275 °C over Ru- or/CeO_2 catalysts except for 0.5%Ru-CeO_2 catalyst. Moreover, the introduction of Ru decreases the catalytic activity of CeO_2 at lower temperature range, especially below 200 °C, and the inhibition effect increases with the increase of Ru content. Our previous studies [27] indicated that the catalytic decomposition of CHCs over Ce based catalysts was related with the concentration of oxygen vacancies (namely Ce^{3+}), which is the main active site adsorbing and dissociating C—Cl bond in CHCs. The introduction of Ru can result in the decrease of the concentration of Ce^{3+}, and hence reduce the catalytic activity to some extent. Additionally, pure CeO_2 and 0.5%Ru-CeO_2 catalysts deactivate significantly above 200 °C, possibly as the result from strong adsorption of HCl or Cl_2 produced during the decomposition of CB on active sites [26]. However, no deactivation of Ru-CeO_2 catalysts with Ru content of 1% or higher was observed (see stability study in details). Thus, it

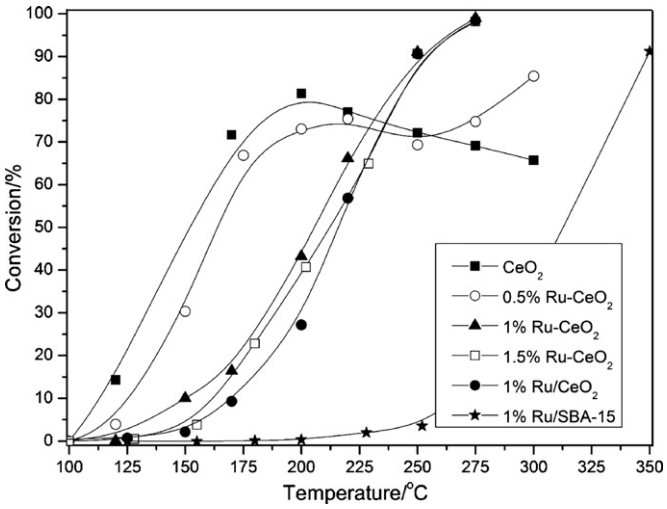

Fig. 6. The light-off curves of CB catalytic combustion over the CeO_2 based catalysts. CB concentration: 550 ppm; GHSV: 15,000 h^{-1}; catalyst amount: 200 mg.

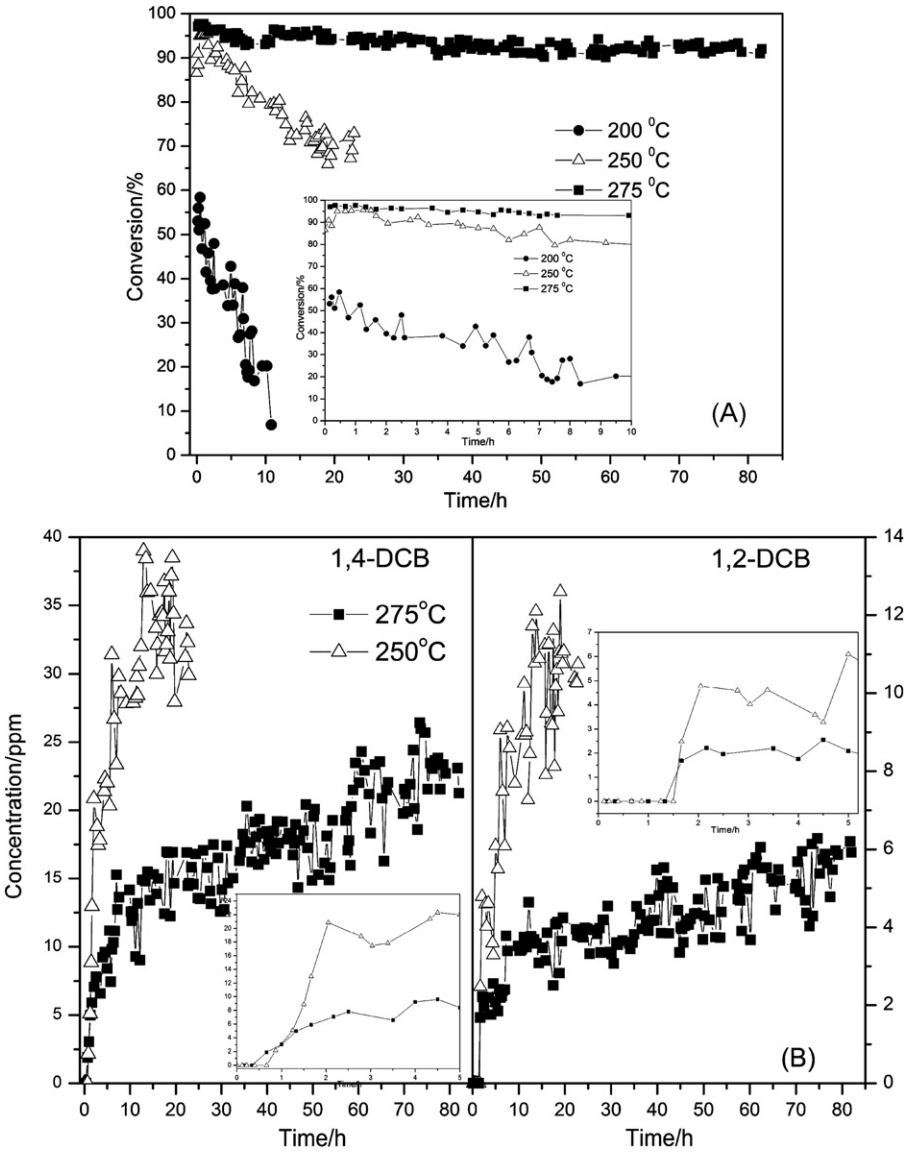

Fig. 7. The stability and by-products of 1%Ru-CeO_2 catalyst for CB catalytic combustion at different temperature. CB concentration: 1500 ppm; GHSV: 15,000 h^{-1}; catalyst amount: 200 mg.

can be speculated that the introduction of Ru into CeO_2 will be favor to improve the stability of Ce-based catalysts.

3.3. Stability studies

Fig. 7 presents the stability and by-products of 1%Ru-CeO_2 catalyst for CB catalytic combustion at different temperature. At 200 °C, CB conversion decreases rapidly from 50% to 20% within 10 h, it can be seen that the stability of 1%Ru-CeO_2 catalyst is not improved essentially at lower temperature compared with pure CeO_2. By raising temperature to 250 °C, deactivation of 1%Ru-CeO_2 catalyst was still observed when conversion of CB decreased gradually from 85% to 70% within 14 h. After that, substantial decrease in CB conversion was not observed. Moreover, it is found that there exists an induction period to obtain the highest activity, the activity increases slowly during the first 0.5–1 h and the conversion increases from the initial value 85–95% after 0.5 h, and then can be maintained at 95% for 1 h (see enlarge figure), and the phenomenon also was observed over the MnO_x/TiO_2 catalyst [56]. As temperature was raised up to 275 °C, CB conversion maintained at 92–95% within 82 h. This phenomenon is consistent with our previous results that there existed a particular temperature above which the ceria catalysts doped with transition metals showed good stability for the CHCs catalytic combustion [2]. In general, chlorine poisoning is one of the main factors to the deactivation of catalysts for CHCs catalytic combustion. Our previous studies indicated that the adsorption of inorganic chlorine species (dissociactive Cl) from the decomposition of CHCs on active sites or surface results in the deactivation of CeO_2 based catalysts, and the removal of these chlorine species is a key step to improve the stability of catalysts. As known, Ru-based catalyst has been applied in industry for large-scale chlorine production via HCl oxidation (Deacon process, the recombination of adjacent dissociated Cl produces Cl_2 over RuO_2) due to its high reactivity and extraordinary stability (limited chlorination and easier Cl_2 removal), and resistant against HCl and Cl_2 exposure. Therefore, it is concluded that Ru species in Ru-CeO_2 catalysts can remove rapidly the dissociacted Cl strongly adsorbed on the active sites via Cl_2, which results in the improvement of CeO_2 stability for CB oxidation. Moreover, the Ru-CeO_2 catalysts have better stability only at higher temperature, which indirectly indicates the importance of Deacon Reaction (lower temperature unfavors HCl oxidation and Cl_2 evolution).

The distribution of chlorinated by-products during stability tests was shown in Fig. 7. None of any by-product is observed at 200 °C, while 1, 4-dichlorobenzene (p-DCB) and 1, 2-dichlorobenzene (o-DCB) are detected when the temperature reaches 250 °C, and their concentration increases slowly with reaction time. Moreover, the amount of DCB at 250 °C is higher than that at 275 °C, probably due to the catalytic decomposition of DCB at higher temperature. The formation of o-DCB (after 1.0 h) is later than p-DCB (see enlarged inset figure), and 1, 3-dichlorobenzene (m-DCB) and other chlorinated by-products are not detected during the stability tests. It is generally considered that DCB compounds can be synthesized by oxychlorination of CB with HCl or chlorination of CB with Cl_2, and the elevated temperature in substitution reactions favors the introduction of a second chlorine atom into the ortho and meta positions, whereas para substitution is favored if cocatalysts and lower temperatures are used [57]. For example, the reaction rate constants of p-DCB, o-DCB and m-DCB prepared by chlorination of CB with Cl_2 are 5.89, 4.16 and 0.2, respectively. Accordingly, the main by-products of CB catalytic combustion over 1%Ru-CeO_2 catalyst are p-DCB and o-DCB. Additionally, Lewis acids ($FeCl_3$, $AlCl_3$, $SbCl_3$, $MnCl_2$, $MoCl_3$, $SnCl_4$ and $TiCl_4$) are used as principal catalysts for the preparation of chlorobenzene or dichlorobenzene in industry, and the formation of p-DCB and o-DCB byproducts may

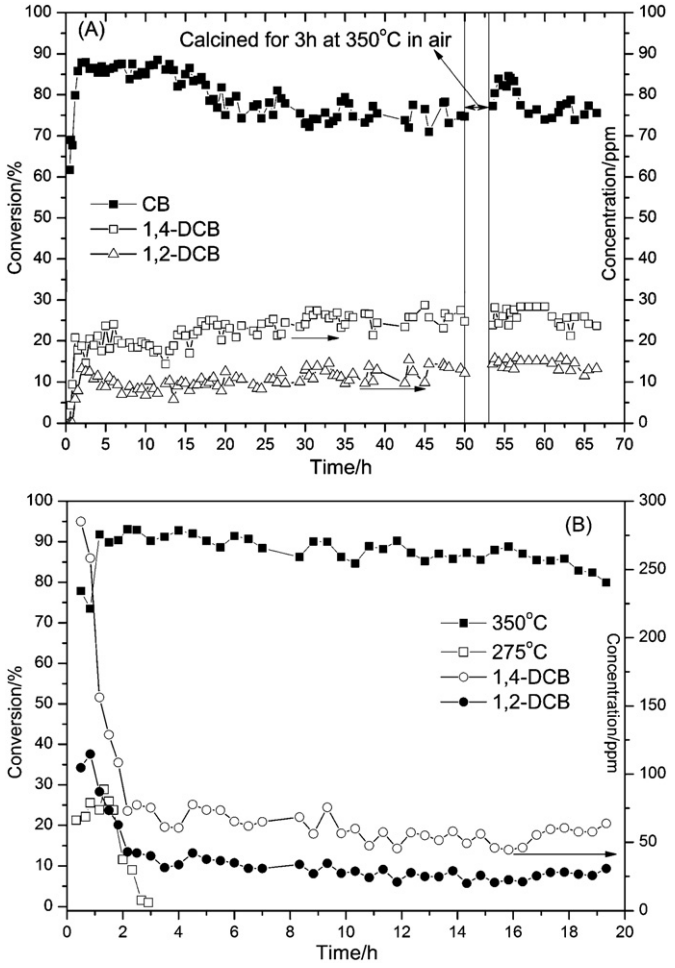

Fig. 8. The stability and distribution of chlorinated products over 1%Ru-CeO_2 and 1%Ru/SBA-15 catalysts for CB catalytic combustion. 1%Ru-CeO_2 (A): CB concentration = 1500 ppm; GHSV = 60,000 h^{-1}; catalyst amount = 50 mg; 1%Ru/SBA-15 (B): CB concentration = 1500 ppm; GHSV = 15,000 h^{-1}; catalyst amount = 100 mg.

be ascribed to the partial chlorination of RuO_2 to RuO_xCl_y or $RuCl_x$ species.

In order to further study and understand the stability of Ru-based catalysts, the stability and by-products of 1%Ru-CeO_2 catalyst under high GHSV (short residence time) condition and 1%Ru/SBA-15 at different temperature for CB catalytic combustion also were investigated and presented in Fig. 8. It can be seen from Fig. 8(A), the CB conversion over 1%Ru-CeO_2 catalyst at 60,000 h^{-1} (catalyst amount is 50 mg) and 275 °C increase rapidly from 60% to 85% within first 1.5 h and demonstrate an obvious induction period. The catalytic activity can be maintained at 85–87% for 17 h, and then decrease slowly to about 71–75% and stable for at least 33 h. The byproducts p-DCB and o-DCB are consistently detected during stability test and the concentration remains at 10–25 ppm. It is worth to note that the selectivity remains constant overtime for the byproducts p-DCB and o-DCB, which suggests clearly that no further deactivation occurred. The initial deactivation observed over is explained by the catalyst chlorination. It follows that the Ru-CeO_2 catalyst still appears better stability for the CB catalytic combustion even under harsh conditions. Additionally, the stability tests of 1%Ru/SBA-15 catalyst at different temperature (see Fig. 8(B)) show that the rapid deactivation can be observed at 275 °C, and the conversion of CB decreases from 30% to 0% within 3 h. Even at higher temperature, such as 350 °C, the catalytic activity only can be remained stable for at most 18 h. It can be considered that the poor stability of 1%Ru/SBA-15 for the CB catalytic combustion

results from the poor activity for the Deacon Reaction, due to the support is critically important for the RuO_2 based catalysts as HCl oxidation [41]. Moreover, no any polychlorinated byproduct is formed at 275 °C due to the absence of Cl_2, by contrast, the byproduct is detected over 1%Ru-CeO_2 catalyst at 250 °C. However, the formation of p-DCB and o-DCB can be observed at 350 °C and the concentration constantly remains at about 60 ppm and 25 ppm within 20 h except the first 2 h, respectively. The phenomenon further indicated that the catalytic activity of HCl oxidation over 1%Ru/SBA-15 is poor at lower temperature.

3.4. TPSR results of 1%Ru-CeO_2 catalysts

The adsorption–desorption behavior of CB and the formation of products, such as DCB, CO_2, H_2O, HCl and Cl_2, over 1%Ru-CeO_2 catalyst were further investigated by TPSR technique. As presented in Fig. 9, the desorption of CB occurs at relatively low temperatures (desorption temperature with maximum is about 130 °C) accompanied with CB decomposition, and the deactivation of catalysts at lower temperature (200 °C) and the formation of DCB at higher temperature (275 °C) are observed by the on-line MS monitoring of CB and DCB, which coincides with the results of stability tests. The formation of CO_2 is detected immediately once the decomposition reaction of CB started, which shows that the CB can be completely oxidized to CO_2 due to the outstanding oxidation performance of Ru-CeO_2 catalysts. By contrast, the evolution of H_2O is later, which probably results from the strong adsorption of H_2O on catalysts surface. Additionally, the reference [36] also found that H_2O evolution was a impeded process during the HCl oxidation to Cl_2 on bulk and supported RuO_2 catalysts and the lower chlorination of TiO_2-R might be due to the difficult desorption of H_2O, which indicated that H_2O desorption was a prominent step. Moreover, the evolutions of Cl_2 and HCl are not observed at 200 °C even after 6 h reaction, it may be due to the strong adsorption of these inorganic chlorine species or dissociative Cl on the CeO_2 surface and the low amount (lower conversion and catalyst deactivation at lower temperature). However, the gaseous Cl_2 and HCl in the effluent can be detected after 3 h at 275 °C, and the amount increases rapidly with the reaction time. After 5.5 h, the amount of Cl_2 and HCl increases slowly and finally reaches constant. These results show that the inorganic chlorine species or dissociatively adsorbed Cl can be removed from the surface of Ru-CeO_2 catalysts at higher temperature, which results in a good stability for CB combustion over the Ru-CeO_2 catalysts. Combining to the stability tests results, the importance of Deacon Reaction for improving the stability of Ru-CeO_2 catalyst can be confirmed, and it can be speculated that Ru-CeO_2 catalyst may be a promising catalyst with higher activity and stability for industrial chlorine recycling. [42]

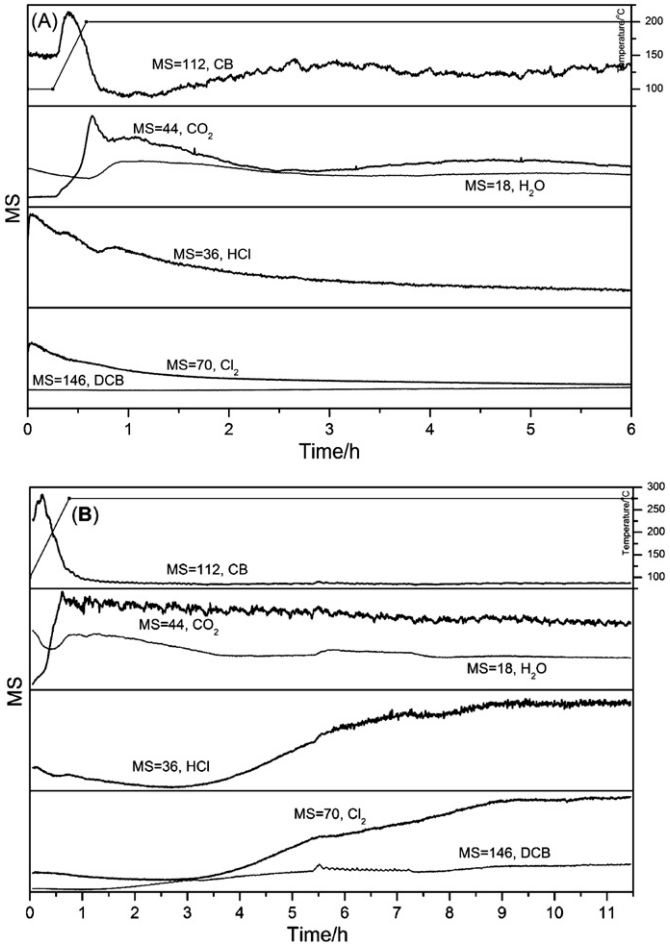

Fig. 9. TPSR profiles for CB decomposition over 1%Ru-CeO_2 catalysts at different temperature: (A) 200 °C, (B) 275 °C. CB concentration: 1500 ppm; GHSV: 15,000 h^{-1}; catalyst amount: 200 mg.

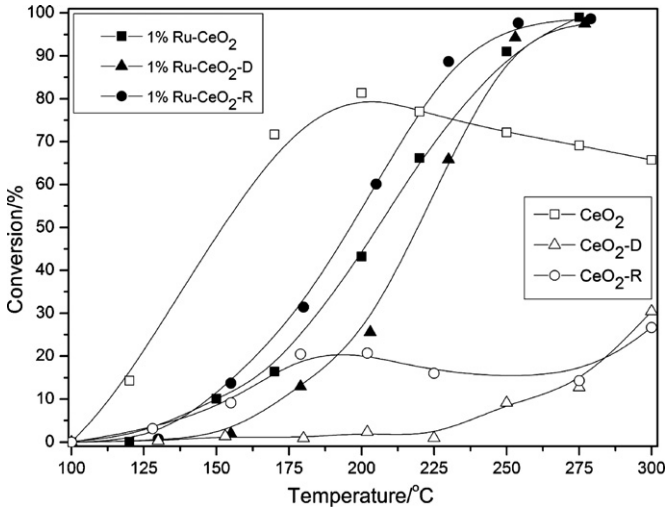

Fig. 10. The light-off curves of CB catalytic combustion over the deactivated and regenerated 1%Ru-CeO_2 and CeO_2 catalysts. Activity evaluation conditions: CB concentration, 550 ppm, GHSV: 15,000 h^{-1}; catalyst amount: 200 mg; deactivated conditions: treated by 15,000 h^{-1} and 3000 ppm CB for 8 h at 200 °C; regenerated conditions: calcined at 300 °C for 3 h in air.

3.5. Catalyst deactivation and regeneration

The catalytic activities for CB catalytic combustion over the deactivated (the fresh catalysts are treated by 15,000 h^{-1} and 3000 ppm CB for 8 h at 200 °C, marked as CeO_2-D and 1%Ru-CeO_2-D) and regenerated (the deactivated catalysts are calcined at 300 °C for 3 h in air, marked as CeO_2-R and 1%Ru-CeO_2-R) 1%Ru-CeO_2 and CeO_2 catalysts were presented in Fig. 10. As shown in Fig. 10, CB conversion over CeO_2-D and CeO_2-R drops dramatically, and the conversion on both catalysts is only 30% even at 300 °C. Moreover, the catalytic activity of CeO_2-R catalyst at low temperature range (125–250 °C) is slightly higher than that the CeO_2-D catalyst, probably due to the removal of a part of chlorine species adsorbed weakly on CeO_2 surface during heat treatment in air [26]. For 1%Ru-CeO_2-D catalyst, CB conversion only slightly decreases comparing with the fresh 1%Ru-CeO_2 catalyst. The temperature for 50% conversion increases from 195 °C to 220 °C, while 90% or higher conversion can be reached at temperature as same as that for the fresh 1%Ru-CeO_2. It seems reasonable to deduce that the deposited chlorine

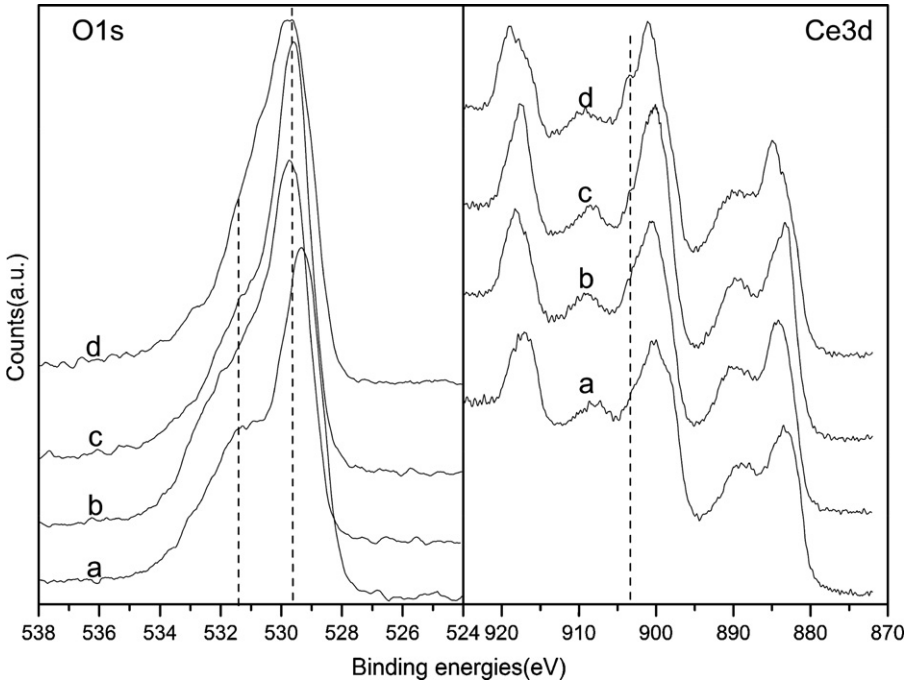

Fig. 11. O1s and Ce 3d XPS spectra of Ru-CeO_2 catalysts: (a) 1%Ru-CeO_2, (b) 1%Ru-CeO_2-D, (c) 1%Ru-CeO_2-R, (d) 1%Ru-CeO_2-82 h.

species can migrate to Ru species at high temperature and then react with oxygen species to form Cl_2 as to remove from the surface of catalysts. It is interesting to find that 1%Ru-CeO_2-R demonstrates higher activity, and the conversion curve shifts to low temperature to some extent. This phenomenon may be related to the induction period observed during stability tests. It is speculated that the reconstruction of catalytic active components or the redistribution of Ru valence state and surface species or changes of the interaction between Ru and CeO_2, and reoxidation of the partially chlorinated catalyst surface, which result in the activity recovery of the regenerated catalyst and the formation of induction period. Additionally, Fig. 8(A) also indicated that, after the stabilized or slightly deactivated 1%Ru-CeO_2 catalyst under high GHSV conditions was calcined for 3 h at 350 °C in air, the catalytic activity was evidently recovered and the conversion of CB increased from 75% to 84%. However, the regenerated catalyst still rapidly deactivated within 3.5 h and then the activity is stable at 70–75%. The results indicated that the partially chlorinated RuO_2 may be the stable active species for the CHCs catalytic combustion, and the rapid deactivation of the regenerated catalyst is ascribed to its easier chlorination due to the re-dispersion of RuO_2 species on CeO_2 surface during heat treatment in air.

In order to further understand the behaviors of Ru-CeO_2 catalysts during CB catalytic combustion, Ru-CeO_2 catalyst treated at different conditions are characterized by XPS technology and the corresponding XPS spectra of O1s and Ce 3d are illustrated in Fig. 11, and the binding energy of Ru 3d is listed Table 2. Comparing with the fresh 1%Ru-CeO_2, O1s peaks at 529.3 eV (assigning to the lattice oxygen species) of samples treated at different conditions shift to higher binding energies, and the shoulder peaks at 531 and 533 eV (assigning to surface adsorbed oxygen species) have obvious decrease. It can be explained as the fact that the adsorption sites of oxygen species are occupied by an amount of inorganic chlorine species (about 3.5–4.1 at%, see Table 2) adsorbed on catalysts surface. Notably, the content of chlorine species on 1%Ru-CeO_2-D (3.73 at%) and 1%Ru-CeO_2-R (3.46 at%) is almost same, which indicates that most of the chlorine species cannot be removed during catalyst regeneration. According to the activity shown in Fig. 10, these residual chlorine species actually do not inhibit CB conversion. Contrarily, the deposition of Cl species on CeO_2, as known, results in the loss in activity. Obviously, these residual Cl species could not reside on Ce species, but on Ru species. Additionally, the Ce 3d XPS spectra (Fig. 11) showed that the content of Ce^{3+} in the treated samples increased by a small extent, especially for the 1%Ru-CeO_2-82h (stability test for 82 h). According to Ru 3d XPS data listed in Table 2, it can be found that the valence of Ru and its relative content are not significantly changed due to the fact that Ru species are stable during CB combustion.

1%Ru-CeO_2-D and -R were analyzed by H_2-TPR tests and the results are presented in Fig. 12. It can be found that the deactivated and regenerated 1%Ru-CeO_2 both show two reduce peaks below 300 °C, are at 115 °C (150 °C) and 205 °C (250 °C), respectively. This feature has been reported elsewhere [58,59]. Madhavaram et al. [58] attributed the high-temperature reduction peak of bulk RuO_2 to an inhibiting influence of water on the reduction kinetics. However, a heterogeneous distribution of RuO_2 particle sizes may also lead to two reduction peaks [59]. The low temperature TPR peak

Table 2
Ru 3d XPS data of 1%Ru-CeO_2 catalysts.

Catalysts	Binding energies (eV)				Ru (at%)		Cl (at%)
	$Ru_{3d5/2}$	$Ru_{3d5/2}$	$Ru_{3d3/2}$	$Ru_{3d3/2}$	~281.8 eV	~282.9 eV	
1%Ru-CeO_2	281.79	283.03	285.85	287.05	0.15	0.12	0.43
1%Ru-CeO_2-82h	281.76	282.98	285.85	287.35	0.14	0.15	4.10
1%Ru-CeO_2-D	281.80	282.90	285.85	287.05	0.14	0.12	3.73
1%Ru-CeO_2-R	281.80	282.93	285.80	286.90	0.14	0.12	3.46

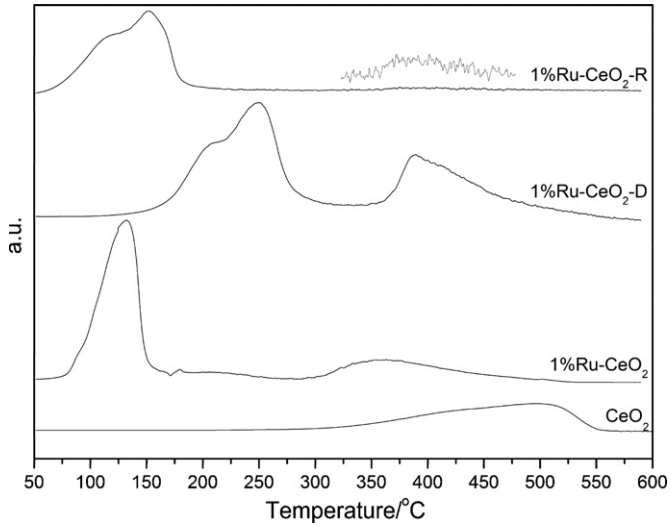

Fig. 12. TPR of the deactivated and regenerated 1%Ru-CeO_2.

can be attributed to reduction of small RuO_2 (well-dispersed) particles, whereas the high-temperature reduction peak can be ascribed to the reduction of larger oxide aggregates (bulk oxide). However, for the fresh 1%Ru-CeO_2 only a peak appears at about 130 °C for reduction of ruthenium oxide. It is speculated that a part of Ru species may migrate to the surface of CeO_2 from the CeO_2 lattice structure during the CB catalytic combustion and highly disperse on the catalyst surface. Therefore, for 1%Ru-CeO_2-D and -R, the new low temperature peaks (115 °C and 205 °C) should be corresponded to highly dispersed ruthenium oxide species. Moreover, the reduction of surface oxygen species of cerium oxide is observed at 350–400 °C. The temperature shifts to high values can be ascribed to the adsorption of inorganic chlorine species or dissociative Cl on catalyst surface (Table 2). Hydrogen consumption for 1%Ru-CeO_2-D is evidently more than that for the fresh and the regenerated 1%Ru-CeO_2 but lower than that for pure CeO_2 (see Table 1). This fact that the reduction peak of 1%Ru-CeO_2-R at this temperature almost disappears indicates that the oxidation treatment for Ru-CeO_2-D favors the migration of surface and lattice oxygen of CeO_2 to Ru species and thus improving redox performance.

3.6. Catalytic activity for other CHCs

The activity of 1%Ru-CeO_2 catalyst for the combustion of TCE, 1, 2-DCE and o-DCB, benzene (B), and the mixture of B and CB are investigated and the results are presented in Fig. 13. Comparing with CB, 1%Ru-CeO_2 catalyst showed poor catalytic activity for the B catalytic combustion, the light-off temperature ($T_{10\%}$) is 190 °C and the conversion only reaches 95% until 300 °C (see Fig. 13(left)). The results can be ascribed to the two reasons presented below: (1) Generally, the dissociation energies for the C—Cl bonds are lower than those for the C—H bonds, and the first step in the catalytic decomposition of CHCs is the splitting of first Cl atom [60]; (2) CeO_2 show outstanding ability of dissociation for the C—Cl bond [25], and the dissociated intermediate species is easily oxidized due to 1%Ru-CeO_2 catalyst possessing excellent oxidation performance. For binary mixtures of CB and B, CB have not been found to obviously influence the conversion of B, especially at low temperature ranges, and the complete combustion temperature ($T_{90\%}$) of B in the mixture were only by ~15 °C higher than when B was oxidized alone. However, the conversion of CB is strongly inhibited by the additive of B, and the $T_{90\%}$ increases from 230 °C to 290 °C. It may be considered that CB catalytic combustion over 1%Ru-CeO_2 catalyst occurs on two types of active sites for dissociation of C—Cl bond and oxidation of the dissociated species, while B catalytic combustion involves only active sites for oxidation. In the presence of both B and CB, CB firstly adsorbs on the dissociation active site of Ru-CeO_2 catalyst, and B is activated mainly on oxidation active sites. The above reaction pathway indicates that the most important role may be a competition between the dissociated CB and B to the oxidation active sites. However, the oxidation active sites are prior occupied by B, accordingly, there will be no effect of CB on B conversion and the conversion of CB will be inhibited by B. Moreover, the inhibition effect of each other at low temperature (lower B and CB conversion) is not distinct, which also indirectly reveals a competition for the same active sites (oxidation active sites), especially at high temperature (the oxidation becomes the rate determining step). Additionally, the slight decrease of B conversion at high

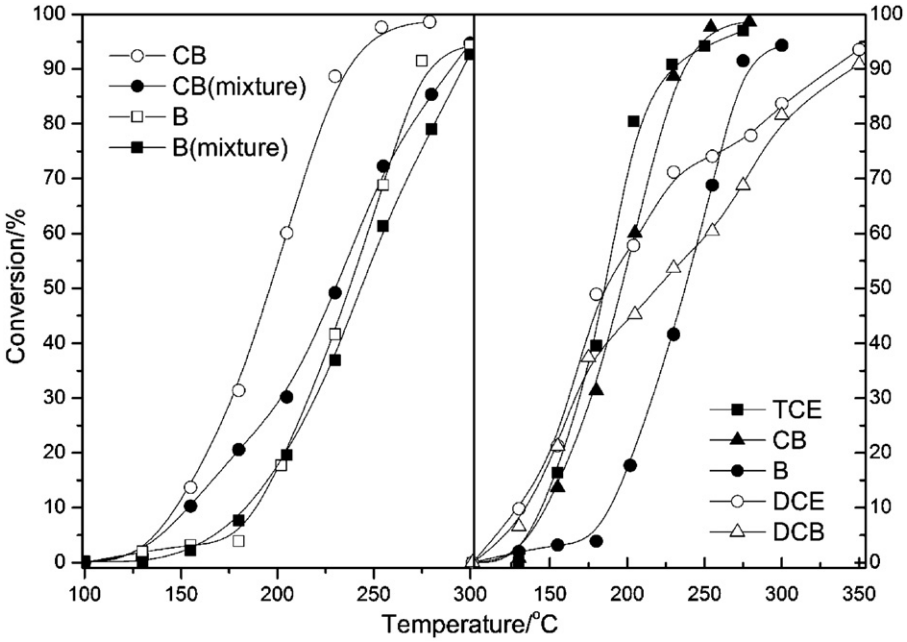

Fig. 13. The light-off curves of catalytic combustion of VOCs over the 1%Ru-CeO_2 catalysts. VOCs concentration: 550 ppm; GHSV: 15,000 h^{-1}; catalyst amount: 200 mg.

temperature can be explained by partial blocking of the active sites on the catalyst surface and the decrease of oxidation ability with strongly adsorbed chlorine species.

Fig. 13 (right) presents the conversion of TCE, 1,2-DCE and o-DCB as a function of temperature over 1%Ru-CeO_2 catalyst, and the activity order is 1,2-DCE > o-DCB > TCE > CB, consistent with the bond dissociation energies (BDE) for C—Cl of 1, 2-DCE, o-DCB, TCE and CB which are 345.1 ± 5.0, 385.8, 391.6 and 399.6 ± 6.3 kJ mol^{-1} [61], respectively. These results further suggest that the rupture of the C—Cl bond is the first step of CHCs catalytic combustion, and is also the rate determining step. However, at above 175 °C, the conversion of 1,2-DCE and o-DCB begins to increase slowly with temperature, and the conversion reaches 90–95% at 350 °C. These phenomena are not completely understood in this study and need to be further investigated, which is beyond the scope of the present manuscript.

4. Conclusions

Ru doped CeO_2 catalysts were prepared by a simple coprecipitation method and characterized by XRD, N_2 adsorption, TEM, Raman, XPS and H_2-TPR. The characterization results indicated that Ru-CeO_2 possesses small particle sizes (~7 nm), high surface area (~105 m^2 g^{-1}) and excellent redox properties. Subsequently, the catalytic combustion of CB and other CHCs, such as TCE, 1,2-DCE and o-DCB was investigated. Compared with Ru/CeO_2 and Ru/SBA-15 catalysts prepared with impregnation method, Ru-CeO_2 catalysts showed more outstanding catalytic activity ($T_{90\%}$ below 250 °C) and stability (at least 82 h at 275 °C) for CB decomposition. The activity order for these CHCs is related to the bond dissociation energies (BDE) for C—Cl in chlorinated organic molecules. The better stability of Ru-CeO_2 catalysts can be ascribed to the fact that inorganic chlorine species (or dissociactive Cl) adsorbed mainly on CeO_2 active sites can be removed rapidly via the Deacon process catalysized by RuO_2 component. Additionally, the activty of the Ru-CeO_2 catalysts deactivated slightly even under harsh conditions (such as high GHSV or low reaction temperature) can be recovered by simple thermal treatment in air. The reaction mechanism of CHCs over Ru-CeO_2 catalysts can be summarized as follows: Firstly, CHCs molecules adsorb on an active sites (mainly CeO_2) where the dissociating and splitting of C—Cl bonds occurs simultaneously. Then, the dissociated CH_x as the indermediate is completely oxidized to H_2O and CO_2 by active oxygen species, but a significant amount of dissociated Cl species still strongly adsorbs on active sites and results in the deactivation of catalysts. However, in the presence of RuO_2, the dissociated Cl can be oxidized rapidly to form Cl_2 via Deacon Reaction and removed from the surface of catalysts or active sites, and the stability of catalysts is improved. Moreover, according to our results and the reference [42], it was speculated that Ru-CeO_2 catalyst may be a promising catalyst with higher activity and stability for industrial chlorine recycling. Although Ru-CeO_2 was found to be a very active and durable catalyst for the catalytic combustion of CHCs, the formation of polychlorinated by-products still was unavoidable. Therefore, further promotion of activity of Ru-CeO_2 catalysts for the Deacon Reaction, such as incorporating Sn or Ti into CeO_2, is a significant topic for further study.

Acknowledgments

The authors would like to thank Wei Deng for preparing TEM and HRTEM samples. This research was supported by National Basic Research Program of China (Nos. 2010CB732300, 2011AA03A406), National Natural Science Foundation of China (No. 20977029) and Commission of Science and Technology of Shanghai Municipality (11JC1402900).

References

[1] H.F. Li, G.Z. Lu, Q.G. Dai, Y.Q. Wang, Y. Guo, Y.L. Guo, ACS Applied Materials & Interfaces 2 (2010) 838–846.
[2] M. Wu, X.Y. Wang, Q.G. Dai, Y.X. Gu, D. Li, Catalysis Today 158 (2010) 336–342.
[3] Y. Dai, X.Y. Wang, Q.G. Dai, D. Li, Applied Catalysis B 111–112 (2011) 141–149.
[4] H.F. Li, G.Z. Lu, Q.G. Dai, Y.Q. Wang, Y. Guo, Y.L. Guo, Applied Catalysis B 102 (2011) 475–483.
[5] Q.Q. Huang, X.M. Xue, R.X. Zhou, Journal of Molecular Catalysis A 344 (2011) 74–82.
[6] B. de Rivas, R. López-Fonseca, M.Á. Gutiérrez-Ortiz, J.I. Gutiérrez-Ortiz, Applied Catalysis B 101 (2011) 317–325.
[7] D. Divakar, M. Romero-Sáez, B. Pereda-Ayo, A. Aranzabal, J.A. González-Marcos, J.R. González-Velasco, Catalysis Today 176 (2011) 357–360.
[8] C. Lucio-Ortiz, J. De la Rosa, A. Ramirez, J. De los Reyes Heredia, P. del Angel, S. Muñoz-Aguirre, L. De León-Covián, Journal of Sol-Gel Science and Technology 58 (2011) 374–384.
[9] C.J. Lucio-Ortiz, J.R. De la Rosa, A. Hernández-Ramírez, E.M. López-Cuellar, G. Beltrán-Pérez, R. del Carmen Miranda Guardiola, C.D. Pedroza-Solís, Colloids and Surfaces A 371 (2010) 81–90.
[10] B. de Rivas, R. López-Fonseca, C. Jiménez-González, J.I. Gutiérrez-Ortiz, Journal of Catalysis 281 (2011) 88–97.
[11] R. Delaigle, P. Eloy, E.M. Gaigneaux, Catalysis Today 175 (2011) 177–182.
[12] K.Y. Jung, Y.R. Jung, J.K. Jeon, J.H. Kim, Y.K. Park, S. Kim, Journal of Industrial and Engineering Chemistry 17 (2011) 144–148.
[13] A.M. Nie, H.S. Yang, Q. Li, X.Y. Fan, F.M. Qiu, X.B. Zhang, Industrial and Engineering Chemistry Research 50 (2011) 9944–9948.
[14] E. Finocchio, G. Ramis, G. Busca, Catalysis Today 169 (2011) 3–9.
[15] M. Piumetti, B. Bonelli, M. Armandi, L. Gaberova, S. Casale, P. Massiani, E. Garrone, Microporous and Mesoporous Materials 133 (2010) 36–44.
[16] L.Y. Jin, R.H. Ma, J.J. Lin, L. Meng, Y.J. Wang, M.F. Luo, Industrial and Engineering Chemistry Research 50 (2011) 10878–10882.
[17] R.H. Ma, P.J. Hu, L.Y. Jin, Y.J. Wang, J.Q. Lu, M.F. Luo, Catalysis Today 175 (2011) 598–602.
[18] Y.L. Gu, Y.X. Yang, Y.M. Qiu, K.P. Sun, X.L. Xu, Catalysis Communications 12 (2010) 277–281.
[19] W. Tian, H.S. Yang, X.Y. Fan, X.B. Zhang, Catalysis Communications 11 (2010) 1185–1188.
[20] T.K. Tseng, L. Wang, C.T. Ho, H. Chu, Journal of Hazardous Materials 178 (2010) 1035–1040.
[21] X.Y. Fan, H.S. Yang, W. Tian, A.M. Nie, T. Hou, F. Qiu, X.B. Zhang, Catalysis Letters 141 (2011) 158–162.
[22] J.F. Lamonier, T.B. Nguyen, M. Franco, S. Siffert, R. Cousin, Y. Li, X.Y. Yang, B.L. Su, J.M. Giraudon, Catalysis Today 164 (2011) 566–570.
[23] C.I. Meyer, A. Borgna, A. Monzón, T.F. Garetto, Journal of Hazardous Materials 190 (2011) 903–908.
[24] X.Y. Wang, Q.G. Dai, Y. Zheng, Chinese Journal of Catalysis 27 (2006) 468–470.
[25] Q.G. Dai, X.Y. Wang, G.Z. Lu, Catalysis Communications 8 (2007) 1645–1649.
[26] Q.G. Dai, X.Y. Wang, G.Z. Lu, Applied Catalysis B 81 (2008) 192–202.
[27] Q.G. Dai, H. Huang, Y. Zhu, W. Deng, S.X. Bai, X.Y. Wang, G.Z. Lu, Applied Catalysis B 117–118 (2012) 360–368.
[28] M. Wu, X.Y. Wang, Q.G. Dai, D. Li, Catalysis Communications 11 (2010) 1022–1025.
[29] Y. Dai, X.Y. Wang, D. Li, Q.G. Dai, Journal of Hazardous Materials 188 (2011) 132–139.
[30] X.Y. Wang, Q. Kang, D. Li, Catalysis Communications 9 (2008) 2158–2162.
[31] J.M. Zhou, L. Zhao, Q.Q. Huang, R.X. Zhou, X.K. Li, Catalysis Letters 127 (2008) 277–284.
[32] Q.Q. Huang, X.M. Xue, R.X. Zhou, Journal of Hazardous Materials 183 (2010) 694–700.
[33] B. de Rivas, R. López-Fonseca, M.Á. Gutiérrez-Ortiz, J.I. Gutiérrez-Ortiz, Catalysis Today 176 (2011) 470–473.
[34] B. de Rivas, R. López-Fonseca, J.R. González-Velasco, J.I. Gutiérrez-Ortiz, Journal of Molecular Catalysis A 278 (2007) 181–188.
[35] S. Pitkääho, L. Matejova, S. Ojala, J. Gaalova, R.L. Keiski, Applied Catalysis B 111–114 (2012) 150–159.
[36] M.A.G. Hevia, A.P. Amrute, T. Schmidt, J. Pérez-Ramírez, Journal of Catalysis 276 (2010) 141–151.
[37] A.P. Amrute, C. Mondelli, M. Moser, G. Novell-Leruth, N. López, D. Rosenthal, R. Farra, M.E. Schuster, D. Teschner, T. Schmidt, J. Pérez-Ramírez, Journal of Catalysis 286 (2012) 287–297.
[38] N. López, J. Gómez-Segura, R.P. Marín, J. Pérez-Ramírez, Journal of Catalysis 255 (2008) 29–39.
[39] A.P. Amrute, C. Mondelli, M.A.G. Hevia, J. Pérez-Ramírez, ACS Catalysis 1 (2011) 583–590.
[40] S. Zweidinger, J.P. Hofmann, O. Balmes, E. Lundgren, H. Over, Journal of Catalysis 272 (2010) 169–175.
[41] J. Pérez-Ramírez, C. Mondelli, T. Schmidt, O.F.K. Schlüter, A. Wolf, L. Mleczk, T. Dreier, Energy & Environmental Science 4 (2011) 4786–4799.
[42] D. Teschner, R. Farra, L.D. Yao, R. Schlögl, H. Soerijanto, R. Schomäcker, T. Schmidt, L. Szentmiklósi, A.P. Amrute, C. Mondelli, J. Pérez-Ramírez, G. Novell-Leruth, N. López, Journal of Catalysis 285 (2012) 273–284.
[43] H. Over, Y.D. Kim, A.P. Seitsonen, S. Wendt, E. Lundgren, M. Schmid, P. Varga, A. Morgante, G. Ertl, Science 287 (2000) 1474–1476.
[44] K. Villani, C.E.A. Kirschhock, D. Liang, G. Van Tendeloo, J.A. Martens, Angewandte Chemie International Edition 45 (2006) 3106–3109.

[45] I. Balint, A. Miyazaki, K.I. Aika, Journal of Catalysis 220 (2003) 74–83.
[46] W.L. Yoon, D.K. Lee, Journal of Chemical Engineering of Japan 37 (2004) 143–151.
[47] D.K. Lee, W.L. Yoon, Catalysis Letters 81 (2002) 247–252.
[48] B. Miranda, E. Díaz, S. Ordóñez, F.V. Díez, Catalysis Communications 7 (2006) 945–949.
[49] S.Y. Mar, C.S. Chen, Y.S. Huang, K.K. Tiong, Applied Surface Science 90 (1995) 497–504.
[50] G. Jacobs, E. Chenu, P. Patterson, L. Williams, D. Sparks, G. Thomas, B. Davis, Applied Catalysis A 258 (2004) 203–214.
[51] X.Y. Wang, J. Ni, B.Y. Lin, R. Wang, J.X. Lin, K.M. Wei, Catalysis Communications 12 (2010) 251–254.
[52] K-D. Schierbaum, Surface Science 399 (1998) 29–38.
[53] C. Korsvik, S. Patil, S. Seal, W.T. Self, Chemical Communications (2007) 1056–1058.
[54] K.S. Kim, N. Winograd, Journal of Catalysis 35 (1974) 66–72.
[55] H.C. Yao, Y.F.Y. Yao, Journal of Catalysis 86 (1984) 254–265.
[56] Y. Liu, M.F. Luo, Z.B. Wei, Q. Xin, P.L. Ying, C. Li, Applied Catalysis B 29 (2001) 61–67.
[57] M. Rossberg, W. Lendle, G. Pfleiderer, Ullmann's Encyclopedia of Industrial Chemistry, Wiley-VCH Verlag GmbH & Co. KGaA, 2000.
[58] H. Madhavaram, H. Idriss, S. Wendt, Y.D. Kim, M. Knapp, H. Over, J. Abmann, E. Löffler, M. Muhler, Journal of Catalysis 202 (2001) 296–307.
[59] I. Balint, A. Miyazaki, K.-i. Aika, Reaction Kinetics and Catalysis Letters 80 (2003) 81.
[60] B. Ramachandran, H.L. Greene, S. Chatterjee, Applied Catalysis B 8 (1996) 157–182.
[61] Y.R. Luo, Handbook of Bond Dissociation Energies in Organic Compounds, CRC Press, Florida, 2002.